高知工科大学
KOCHI UNIVERSITY OF TECHNOLOGY

Versatility of One-pot, Single-step Synthetic Approach for Spherical Porous (Metal) Oxide Nanoparticles Using Supercritical Alcohols

著者	Wang Pengyu, Ueno Kimiyoshi, Takigawa Hikaru, Kobiro Kazuya
journal or publication title	The Journal of Supercritical Fluids
volume	78
page range	124-131
year	2013
URL	http://hdl.handle.net/10173/1361

doi: 10.1016/j.supflu.2013.03.023

Versatility of One-pot, Single-step Synthetic Approach for Spherical Porous (Metal) Oxide Nanoparticles Using Supercritical Alcohols

Pengyu Wang*, Kimiyoshi Ueno, Hikaru Takigawa, Kazuya Kobiro*

School of Environmental Science and Engineering, Kochi University of Technology, 185 Miyanokuchi, Tosayamada, Kochi 782-8502, Japan

Graphical abstract

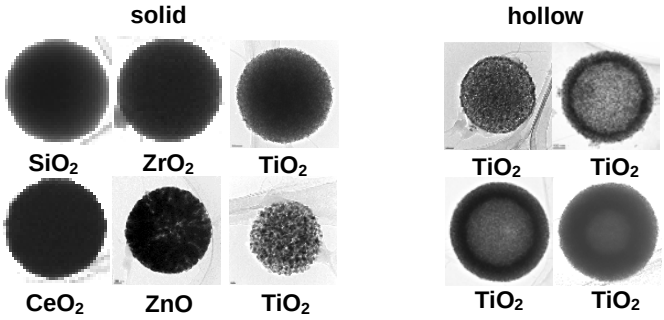

*Corresponding author. Tel.: +81 887 57 2503; fax: +81 887 57 2520.

E-mail address: wang.pengyu@kochi-tech.ac.jp (P. Wang);

kobiro.kazuya@kochi-tech.ac.jp (K. Kobiro)

ABSTRACT

We developed a rapid, one-pot, single-step synthetic method for preparing spherical porous (metal) oxides, titanium dioxide, silica, zirconium dioxide, cerium dioxide, and zinc oxide with large surface areas in a supercritical alcohol containing formic acid or phthalic acid as organic additive in a very short reaction time (10 min). A new type of hollow TiO_2 nanoparticle was obtained by slowly heating the reaction mixtures. The shell thickness of hollow TiO_2 nanoparticles was controlled by adjusting the heating rate. The method proved highly versatile for synthesizing solid and hollow spherical meso/microporous nanoparticles. The spherical mesoporous TiO_2 nanoparticles photocatalytically degraded methylene blue in water under UV irradiation, and successfully transported DNA under biolistic bombardment.

Keywords: Hollow and solid spherical meso/microporous, (Metal) oxide, One-pot, Single-step, Supercritical alcohol

1. Introduction

Porous materials such as zeolites [1-3], metal organic frameworks [4-6], and metal oxides [7-10] are characterized by large surface areas and controlled pore dimensions. Consequently, they have attracted substantial attention in the fields of gas absorption, separation, condensation, drug delivery, and substrate-size-controlled catalysis [1-10]. Among them, metal oxide nanoparticles, such as silica (SiO_2) [11-13], titanium dioxide (TiO_2) [14-17], cerium dioxide (CeO_2) [18-20], zirconium dioxide (ZrO_2) [21,22], and variants of these [23], are of particular relevance to catalytic chemistry, semiconductors, and drug delivery. Porous metal oxide nano- or micro-spheres with dimension-controlled morphology possess unique properties that are especially suited to practical applications. These properties include easy manipulation, effective catalyst recovery, excellent thermal stability, monodisperse nature, and exceptional light-harvesting properties [24-26]. We have designated such meso/microporous nanospheres as **m**eso/**m**icroporously **a**rchitected **r**oundly **i**ntegrated **m**etal **o**xide (MARIMO) nanoparticles, because their shapes resemble those of *MARIMO* (*Cladophora aegagropila*) moss balls. Several methods exist by which to obtain these structures, including hydrothermal, sol-gel, and self-assembly methods, and combinations of these. However, these methods generally involve complex multistep

operations and long reaction times (several hours) [1-13,14-23,27,28]. Recently, size- and morphology-controlled inorganic–organic hybrid metal and metal oxide nanoparticles have been synthesized in supercritical fluids. Supercritical ethanol (scEtOH) yields monodisperse metal nanoparticles [29], supercritical methanol (scMeOH) [30,31] or supercritical water (SCW) [32] yields zinc oxide (ZnO) nanoparticles, while SCW alone yields CeO_2 [33], TiO_2 [34], and magnetite (Fe_3O_4) [35] nanoparticles. All of these reactions proceed in a short reaction time (several seconds to several minutes) [36-41]. However, a versatile synthetic method for MARIMO nanoparticles in supercritical fluids has yet to be established.

Fig. 1

Very recently, we developed a one-pot, single-step method that synthesizes a series of spherical mesoporous TiO_2 nanoparticles with large specific surface areas. The reaction mixture comprises scMeOH in the presence of a carboxylic acid, and the reaction is completed within several minutes (Fig. 1) [14]. The particle and pore sizes of the MARIMO TiO_2 are controlled by changing the reaction temperature (Fig. 1a and b). In addition, by merely changing the carboxylic acid, both solid and hollow MARIMO TiO_2 are produced (Fig. 1c). In this paper, we show that the synthetic approach can yield a variety of other (metal) oxide nanospheres such as SiO_2, CeO_2, ZrO_2, and ZnO. The

method can also synthesize a new type of hollow MARIMO TiO_2 nanosphere with thickness-controllable shell.

2. Materials and methods

2.1 General information

Ethanol, methanol, phthalic acid, formic acid, acetic acid, tetraethyl orthosilicate, zirconium oxynitrate dihydrate, cerium (III) nitrate hexahydrate, titanium tetraisopropoxide, zinc acetate dihydrate, and methylene blue were purchased from Wako Pure Chemical Industries Co. Ltd. They were used as received without further purification.

2.2 Characterization

X-ray diffraction (XRD) patterns were obtained using Rigaku SmartLab with graphite-monochromatized Cu $K\alpha$ radiation. Transmission electron microscope (TEM) and high-resolution transmission electron microscopy (HRTEM) images were taken using JEOL JEM-2100F. Field emission scanning electron microscope (FESEM) images were taken on JEOL JSM7300F. Fourier transform infrared (FTIR) spectra were obtained using JASCO FT/IR-4200 (type A). Dynamic light scattering (DLS) analyses were performed using a Photal FPAR-1000 Fiber-Optics Particle Analyzer. Nitrogen adsorption–desorption isotherm spectra were obtained using BEL Japan INC Belsorp II and Brunauer-Emmett-Teller (BET) specific surface areas were obtained using BET

Shimadzu FlowSorb II 2300. Ultraviolet visible absorption (UV-vis) spectra of the nanoparticles were obtained using JASCO V-670.

2.3 Preparation of mesoporous nanoparticles

A metal salt (2 mmol) was added to a solution of carboxylic acid in 20 mL of methanol or ethanol (0.5 mol L^{-1}), with vigorous stirring.

Synthesis of spherical meso/microporous (metal) oxide nanoparticles in supercritical alcohols by rapid heating: The MeOH or EtOH solution (3.5 mL) was transferred into an SUS 316 batch-type reactor (10 mL volume). The reactor was sealed with a screw cap equipped with a thermocouple for measuring the inner reactor temperature. The reactor was then placed in a molten salt bath maintained at an appropriate temperature, and heated for an appropriate time. The reaction was quenched by placing the reactor into an ice-water bath. The screw cap was opened after the reactor had cooled completely. The crude product was sonicated in MeOH or EtOH (30 min) and centrifuged (6600 rpm, 10 °C, and 30 min). The upper layer was decanted. This procedure was undertaken three times. The obtained powdery product was vacuum-dried at 30 °C for 24 h.

Synthesis of spherical mesoporous metal oxide nanoparticles in supercritical alcohols by slow heating: The reactor was heated from 30 °C to an appropriate temperature at an appropriate heating speed in a gas chromatography oven. After reaction, the reactor was cooled at an appropriate rate or placed into an ice-water bath.

2.4 Photocatalytic degradation of methylene blue

MARIMO TiO_2 nanoparticles were calcined at 500 °C for 60 min to remove surface organic materials. The MARIMO TiO_2 nanoparticles (5 mg) were dispersed in 5 mL of methylene blue water solution (1.0×10^{-5} mol L^{-1}). The photocatalytic degradation was performed in a quartz cell irradiated by a 300 W xenon light source (Asahi spectra, MAX-301). Light of wavelength longer than 370 nm was removed by an optical filter. Following irradiation for an appropriate time, the catalyst was removed by a membrane filter (Millipore, MILLEX-HV 0.45 μm Filter Unit) and the absorption spectra of the filtrate were measured on a UV-vis spectrophotometer (JASCO V-560).

3. Results and discussion

Microporous SiO_2 nanospheres were obtained by reacting tetraethoxysilane in scEtOH (0.28 g mL^{-1}) at 400 °C for 10 min in the presence of phthalic acid. This reaction yielded a white powder; however, a similar reaction using scMeOH yielded very few particles. From field emission scanning electron microscopy (FESEM) and transmission electron microscopy (TEM) images, the particles obtained in scEtOH are seen to possess the characteristic MARIMO morphology (Fig. 2a, 2b, and S1). Broad peaks observed in the powder XRD pattern of the particles clearly indicate their amorphous SiO_2 nature (Fig. 3a) [42]. The average size of the MARIMO SiO_2 particles obtained at 400 °C is 1316 ± 305 nm (dynamic light scattering (DLS) measurements; Fig. S2) and the particle size distribution is very narrow. The Brunauer–Emmett–Teller (BET) specific surface area density of the MARIMO SiO_2 nanoparticles is 715 m^2 g^{-1}, larger than some of the reported and commercially available MARIMO SiO_2 microspheres [11-13]. The nitrogen adsorption–desorption isotherm of the MARIMO SiO_2 microparticles is of type I, indicating that the synthesized MARIMO SiO_2 microparticles are microporous (Fig. 4a and b). To examine whether surface organic residues exist on the MARIMO SiO_2 microparticles, Fourier transform infrared (FTIR) reflection spectra were acquired (Fig. S3). A broad absorption appeared at 3700–3000

cm^{-1}, consistent with hydrogen-bonded O–H stretching on the surface of the SiO_2 microparticles and/or absorbed H_2O. The absorptions at 2975 and 2894 cm^{-1} are attributable to C–H stretching vibrations of the organic compounds on the SiO_2 surface. The absorptions at 1650–1550 and 1409 cm^{-1} correspond to absorptions of the carboxylate (COO^-) group, indicating that phthalic acid is attached to the surface of the MARIMO SiO_2 microparticles. These results indicated that the carboxylic acid could interconnect the primary particles of MARIMO nanoparticles and/or simply cover the surface of the primary particles. The broad, intense bands appearing at 1087 and 800 cm^{-1} correspond to the symmetric stretching vibration of Si–O–Si, while the sharp peak at 970 cm^{-1} corresponds to Si–OH [43,44].

Fig. 2

Fig. 3

Fig. 4

The one-pot, one-step supercritical alcohol method was then applied to the synthesis of MARIMO ZrO_2 and CeO_2 nanoparticles. Each of these particles was readily obtained by exposing the corresponding metal salt ($ZrO(NO_3)_2 \cdot 2H_2O$ or $Ce(NO_3)_3 \cdot 6H_2O$, respectively) to formic acid in scMeOH (0.28 g mL^{-1}). The reaction proceeded at 300 °C for 10 min. TEM images of ZrO_2 (Fig. 2c and d) and CeO_2 (Fig. 2e and f)

nanoparticles indicate that all of the obtained nanoparticles possess the MARIMO morphology. XRD diffraction patterns revealed the crystal structures of the nanoparticles as tetragonal for ZrO_2 and cubic for CeO_2 (Fig. 3b and c). From dynamic light scattering (DLS) measurements, the average diameters of the nanoparticles were determined as 485 ± 274 nm (Fig. S9a) and 1190 ± 854 nm (Fig. S15a) for ZrO_2 and CeO_2, respectively. The respective BET specific surface area densities are 228 $m^2\ g^{-1}$ and 34 $m^2\ g^{-1}$. The nitrogen adsorption–desorption isotherms of the MARIMO ZrO_2 and CeO_2 nanoparticles were of types I and IV, respectively, indicating that the MARIMO ZrO_2 nanoparticles are microporous (Fig. 4c and d) and the MARIMO CeO_2 nanoparticles are mesoporous (Fig. 4e and f). A higher reaction temperature (400 °C) yielded slightly smaller MARIMO nanoparticles of ZrO_2 (428 ± 236 nm, Fig. S9b) and CeO_2 (653 ± 326 nm, Fig. S15b) with reduced specific surface area (154 and 31 $m^2\ g^{-1}$, respectively). A similar procedure easily afforded divalent metal oxide, MARIMO ZnO, nanoparticles (Fig. S16-S19). These results confirm the successful fabrication of MARIMO TiO_2 [14], SiO_2, ZrO_2, CeO_2, and ZnO. Thus, the simple one-pot, one-step reactions of (metal) salts in the presence of carboxylic acids in supercritical alcohols is available means of obtaining spherical porous nanoparticles within a few minutes.

Rapidly heating a reaction mixture comprising $Ti(O^iPr)_4$, formic acid, and MeOH to 400 °C (within 30 s) yields well-formed hollow TiO_2 nanospheres with a very thin shell as reported before (Fig. 1c) [14]. In the current study, we synthesized another type of hollow MARIMO TiO_2 nanoparticle, whose shell thickness was controlled by tuning the heating rate of the reaction. Slowly heating a reaction mixture of $Ti(O^iPr)_4$, phthalic acid, and MeOH from room temperature to 300 or 400 °C (ca. 5.4 °C/min) produced well-formed hollow MARIMO anatase TiO_2 nanoparticles with a thick shell (thickness 140 and 105 nm [45], respectively; Fig. 5a-d and 6a; 5e-h and 6b).The hollow structures of the nanoparticles were directly confirmed by FESEM images of broken particles (Fig. 5b and 5f). The lower temperature (300 °C) resulted in small-sized primary nanoparticles (Fig. 5d), while the higher temperature (400 °C) yielded larger ones (Fig. 5h), consistent with the results for solid MARIMO TiO_2 nanospheres [14]. Moreover, lowering the reaction temperature to 200 °C yielded hollow MARIMO amorphous TiO_2 (Fig. S30 and S31). The specific surface area of the hollow MARIMO TiO_2 nanoparticles obtained at 300 °C is 178 $m^2\ g^{-1}$, and their structures contain mesopores (Fig. S25). In addition, slower heating (ca. 2 °C/min) provided hollow MARIMO anatase TiO_2 nanoparticles with a thicker shell (281 nm [45]; Fig. 5i-l and 6c). More rapid heating (ca. 10 °C/min) reduced the shell thickness to 120 nm [45] (Fig. 5m-p, 6d).

Thus, the hollow MARIMO morphology depends critically on heating rate; however, slow cooling from higher temperatures exerted no effect on MARIMO morphology (where slow cooling denotes ca. 5.4 °C/min from 300 °C (Fig. S23 and S24) and ca. 5.4 °C/min from 400 °C (Fig. S27 and 28)). MARIMO structure was also independent of reaction time (10, 30, and 60 min) at 300 °C and 0.28 g mL^{-1} MeOH density (Fig. 1a, S20 and S21). Hollow mesoporous TiO_2 nanoparticles with controllable shell thickness have recently been synthesized using a SiO_2 microsphere template [15]. While this approach is interesting and novel, our approach is considerably simpler, since ours controls shell thickness and pore size of hollow TiO_2 nanoparticles by merely changing heating rate in a one-pot single-step reaction.

Fig. 5

Fig. 6

The formation mechanisms of MARIMO nanoparticles were investigated by modifying the reaction conditions [46]. First, MeOH was replaced with 2-propanol as solvent in the reaction of $Ti(O^iPr)_4$ with phthalic acid or HCOOH under similar reaction conditions. However, dispersed single TiO_2 crystals rather than MARIMO TiO_2 were obtained in both reactions (Fig. S34). The presence of carboxylic acid is also important. When the reaction was executed in scMeOH without carboxylic acid, aggregated single

crystals again resulted (Fig. S36), whereas MARIMO nanoparticles always formed in the presence of acid (Fig. S37 and S38). Moreover, pore sizes of the MARIMO TiO_2 nanoparticles increased at higher concentrations of carboxylic acid (Fig. S37 and S38). Thus, the combination of scMeOH and carboxylic acid is crucial for the formation of the MARIMO nanoparticles.

Based on these results, we have proposed a carboxyl-group-assisted process for the formation of solid MARIMO nanoparticles (Scheme 1, rapid heating) [14]; substitution of sterically bulky isopropoxy groups by less-bulky methoxy groups forms primitive titanium alkoxide oligomers by transesterification at high temperature in the presence of carboxylic acid in methanol [47]. Under these conditions, some of the primitive oligomers are interconnected via surface interactions with carboxyl groups. As the reaction mixture is heated further, esterification of acids with methanol proceeds easily with water formation. The titanium alkoxide oligomers bearing carboxylic acids react with the water to form TiO_2 crystals [28]. Parallel decomposition of the carboxylic acid evolves gaseous products such as CO_2 and hydrocarbons. These processes occur rapidly under rapid heating (within 30 sec), with consequent expansion of the nanospheres to ultimately yield either solid or thin-shelled hollow MARIMO nanoparticles (Scheme 1, rapid heating). On the other hand, hollow thick-shelled MARIMO nanoparticles are

formed under slow heating rate by the Ostwald ripening effect (Scheme 1, slow heating) [48,49]. Since low reaction temperature (200 °C) resulted in amorphous MARIMO TiO_2 and slower heating rate increased the shell thickness of the nanospheres, we infer that amorphous TiO_2 generated first at low temperature becomes crystalline with rising temperature concomitant with the Ostwald ripening effect. Poorly-formed crystals are lost, resulting in larger and more complete single crystals with thick-shelled hollow MARIMO morphology. Slower heating also enhances the Ostwald ripening effect that favors the hollow MARIMO morphology with larger primary particles, as well as thicker shell wall.

Scheme 1.

To assess the efficacy of MARIMO TiO_2 as a photocatalytic material, we tested its ability to degrade methylene blue in water. The MARIMO TiO_2 nanoparticles used for this purpose were obtained in the presence of phthalic acid in scMeOH (0.28 g mL^{-1}) at 300 °C (reaction time 10 min; Fig. 1a). The UV-vis spectrum of the particles is shown in Fig. S39. The MARIMO TiO_2 nanoparticles absorbed light at wavelengths shorter than 400 nm. The nanoparticles were dispersed throughout the methylene blue water solution. Fig. 7 illustrates the degradation of methylene blue in the presence of MARIMO TiO_2 nanoparticles under irradiation by 370 nm UV light. The solution became colorless after

10 min, indicating that the MARIMO TiO_2 nanoparticles can properly degrade methylene blue under UV irradiation (370 nm). Although the specific surface area of MARIMO TiO_2 is larger than that of commercially available P25, the reaction rate (k_f = 2.9×10^{-1} min^{-1}) of photodegradation by MARIMO TiO_2 as a catalyst was smaller as compare to that by commercially available P25 (k_f = 1.52 min^{-1}, Fig. S40). It can be due to inside of MARIMO TiO_2 is not available effectively, since light could not penetrate deeply inside of MARIMO TiO_2 and/or methylene blue did not diffuse inside. Only surface of MARIMO, namely, can be used efficiently in this reaction.

Fig. 7

Moreover, the MARIMO TiO_2 nanoparticles were successfully applied as a new material for transporting DNA under biolistic bombardment [50]. The current gold or tungsten nanoparticles used for biolistic bombardment are classified as nano-aggregates, with average aggregation sizes of several hundred nanometers. Our MARIMO TiO_2 nanoparticles possess size-controlled complete spherical structure with numerous mesopores which can readily admit plasmids. The MARIMO TiO_2 nanoparticles shown in Fig. 1a were used for this purpose. The MARIMO TiO_2 nanoparticles were mixed with supercoiled pHyg3 plasmid carrying the hygromycin resistance gene aphVII. The particles were shot into *Chlamydomonas reinhardtii* cells by high pressure He gas (7.6

MPa). After two weeks, colonies appeared on hygromycin-infused agar plates, confirming that the novel MARIMO TiO_2 nanoparticles had successfully transported DNA under biolistic bombardment (Fig. 8). Thus, the MARIMO TiO_2 nanoparticles delivered the DNA despite their reduced density and can replace the heavy, expensive gold and tungsten nanoparticles currently used in DNA transport.

Fig. 8

4. Conclusions

Meso/microporously architected roundly integrated (metal) oxide (MARIMO) TiO_2, SiO_2, ZrO_2, CeO_2, and ZnO nanoparticles with large surface areas were successfully synthesized by a simple one-pot, one-step synthetic approach in the presence of carboxylic acids (phthalic acid and formic acid) as organic additives in supercritical alcohols. The reaction proceeds over a short time scale. A new type of hollow TiO_2 nanoparticle resulted from slow heating of the reaction mixtures. The thickness of the shell can be controlled by adjusting the heating rate. The one-pot, one-step synthetic method was extremely versatile, yielding a series of solid and hollow MARIMO nanoparticles. The synthesized MARIMO TiO_2 nanoparticles were successfully applied to two practical situations; UV-assisted photocatalytic degradation of methylene blue in water, and DNA transport under biolistic bombardment.

Acknowledgements

The authors gratefully acknowledge Mr. Masao Yamashita and Dr. Tsutomu Nakanishi of Kagawa Industry Support Foundation for the synthesis of hollow MARIMO TiO_2 nanoparticles. The authors extend their sincere thanks to Prof. Tomoya Konishi of Anan National College of Technology for FTIR analyses. The authors are sincerely grateful to Prof. Hiromichi Aono of Ehime University for the BET and nitrogen adsorption–desorption isotherm spectra. The authors thank Prof. Nagatoshi Nishiwaki and Dr. Noriko Nitta of Kochi University of Technology for their fruitful discussions. The authors also thank Mr. Tetsuo Nagayama and Mr. Masato Sato of social cooperation division of Kochi University of Technology for their support.

References

[1] H. Chen, J. Wydra, H. Zhang, P.-S. Lee, Z. Wang, W. Fan, M. Tsapatsis, Hydrothermal synthesis of zeolites with three-dimensionally ordered mesoporous-imprinted structure, J. American Chemical Society 133 (2011) 12390-12393.

[2] Q. Meng, D.C. Doetschman, A.K. Rizos, M.-H. Lee, J.T. Schulte, A. Spyros, C.W. Kanyi, Adsorption of organophosphates into microporous and mesoporous NaX zeolites and subsequent chemistry, Environmental Science Technology, 45 (2011) 3000-3005.

[3] J. Zhao, J. Zhou, Y. Chen, Q. He, M. Ruan, L. Guo, J. Shi, H. Chen, Fabrication of mesoporous zeolite microspheres by a one-pot dual-functional templating approach, J. Materials Chemistry, 19 (2009) 7614-7616.

[4] S. Xiang, Y. He, Z. Zhang, H. Wu, W. Zhou, R. Krishna, B. Chen, Microporous metal-organic framework with potential for carbon dioxide capture at ambient conditions, Nature Communications, DOI: 10.1038/ncomms1956.

[5] N. Stock, S. Biswas, Synthesis of Metal-Organic Frameworks (MOFs): Routes to various MOF topologies, morphologies, and composites, Chemical Reviews 112 (2012) 933-969.

[6] M. Yoon, R. Srirambalaji, K. Kim, Homochiral metalorganic frameworks for asymmetric heterogeneous catalysis, Chemical Reviews 112 (2012) 1196-1231.

[7] X. Sun, Y. Shi, P. Zhang, C. Zheng, X. Zheng, F. Zhang, Y. Zhang, N. Guan, D. Zhao, G.D. Stucky, Container effect in nanocasting synthesis of mesoporous metal oxides, J. American Chemical Society 133 (2011) 14542-14545.

[8] W. Cai, J. Yu, C. Anand, A. Vinu, M. Jaroniec, Facile synthesis of ordered mesoporous alumina and alumina-supported metal oxides with tailored adsorption and framework properties, Chemistry of Materials 23 (2011) 1147-1157.

[9] N.C. Strandwitz, G.D. Stucky, Hollow Microporous cerium oxide spheres templated by colloidal silica, Chemistry of Materials 21 (2009) 4577-4582.

[10] X. Liang, M. Yu, J. Li, Y.-B. Jiang, A.W. Weimer, Ultra-thin microporous–mesoporous metal oxide films prepared by molecular layer deposition (MLD), Chemical Communications (2009) 7140-7142.

[11] F. Tang, L. Li, D. Chen, Mesoporous silica nanoparticles: synthesis, biocompatibility and drug delivery, Advanced Materials 24 (2012) 1504-1534.

[12] Y.L. Choi, J.H. Lee, J. Jaworski, J.H. Jung, Mesoporous silica nanoparticles functionalized with a thymidine derivative for controlled release, J. Materials Chemistry 22 (2012) 9455-9457.

[13] P. Yang, S. Gai, J. Lin, Functionalized mesoporous silica materials for controlled drug delivery, Chemical Society Reviews, 41 (2012) 3679-3698.

[14] P. Wang, K. Kobiro, Ultimately simple one-pot synthesis of spherical mesoporous TiO_2 nanoparticles in supercritical methanol, Chemistry Letters 41 (**2012)** 264-266.

[15] J.B. Joo, Q. Zhang, I. Lee, M. Dahl, F. Zaera, Y. Yin, Mesoporous anatase titania hollow nanostructures though silica-protected calcination, Advanced Functional Materials 22 (2012) 166-174.

[16] M.P. Hong, J.Y. Kim, K. Vemula, H.S. Kim, K.B. Yoon, Synthesis of monodisperse mesoporous TiO_2 spheres with tunable sizes between 0.6 and 3.1 lm and effects of reaction temperature, Ti source purity, and type of alkylamine on size and monodispersity, Chemical Communications 48 (2012) 4250-4252.

[17] Z. Sun, J.H. Kim, Y. Zhao, F. Bijarbooneh, V. Malgras, Y. Lee, Y.-M. Kang, S.X. Dou, Rational design of 3D dendritic TiO_2 nanostructures with favorable architectures, J. American Chemical Society 133 (**2011)** 19314-19317.

[18] J. Wei, Z. Yang, Y. Yang, Fabrication of three dimensional CeO_2 hierarchical structures: precursor template synthesis, formation mechanism and properties, CrystEngComm 13 (2011) 2418-2424.

[19] Z. Yang, J. Wei, H. Yang, L. Liu, H. Liang, Y. Yang, Mesoporous CeO_2 hollow spheres prepared by Ostwald ripening and their environmental applications, European J. Inorganic Chemistry (2010) 3354-3359.

[20] T. Brezesinski, J. Wang, R. Senter, K. Brezesinski, B. Dunn, S.H. Tolber, On the correlation between mechanical flexibility, nanoscale structure, and charge storage in periodic mesoporous CeO_2 thin films, *ACS Nano.* 4 (2010) 967-977.

[21] Y. Chen, S.K. Lunsford, Y. Song, H. Ju, P. Falaras, V. Li-kodimos, A.G. Kontos, D.D. Dionysiou, Synthesis, characterization and electrochemical properties of mesoporous zirconia nanomaterials prepared by self-assembling sol–gel method with Tween 20 as a template, Chemical Engineering J. 170 (2011) 518-524.

[22] A. Mondal, A. Zachariah, P. Nayak, B.B. Nayak, Synthesis and room temperature photoluminescence of mesoporous zirconia with a tetragonal nanocrystalline framework, J. American Ceramic Society 93 (2010) 387-392.

[23] X. Lai, J. Li, B. A. Korgel, Z. Dong, Z. Li, F. Su, J. Du, D. Wang, General synthesis and gas-sensing properties of multiple-shell metal oxide hollow microspheres, Angewandte Chemmie International Edition 50 (2011) 2738-2741.

[24] S. Liu, J. Yu, M. Jaroniec, Tunable photocatalytic selectivity of hollow TiO_2 microspheres composed of anatase polyhedra with exposed {001} facets, J. American Chemical Society 132 (2010) 11914-11916.

[25] X. Hu, G. Li, J.C. Yu, Design, fabrication, and modification of nanostructured semiconductor materials for environmental and energy applications, Langmuir 26 (2009) 3031-3039.

[26] J.H. Pan, X. Zhang, A.J. Du, D.D. Sun, J.O. Leckie, Self-etching reconstruction of hierarchically mesoporous F-TiO_2 hollow microspherical photocatalyst for concurrent membrane water purifications, J. American Chemical Society 130 (2008) 11256-11257.

[27] A.A. Ismail, D.W. Bahnemann, Mesoporous titania photocatalysts: preparation, characterization and reaction mechanisms, J. Materials Chemistry 21 (2011) 11686-11707.

[28] X. Chen, S.S. Mao, Titanium dioxide nanomaterials: synthesis, properties, modifications, and applications, Chemical Reviews 107 (2007) 2891-2959.

[29] S.K. Pahari, T. Adschiri, A.B. Panda, Synthesis of monodispersed nanocrystalline materials in supercritical ethanol: a generalized approach, J. Materials Chemistry 21 (2011) 10377-10383.

[30] A.A. Vostrikov, O.N. Fedyaeva, A.V. Shishkin, M.Ya. Sokol, ZnO nanoparticles formation by reactions of bulk Zn with H_2O and CO_2 at sub- and supercritical conditions: I. Mechanism and kinetics of reactions, J. Supercritical Fluids 48 (2009) 154-160.

[31] A.A. Vostrikov, O.N. Fedyaeva, A.V. Shishkin, M.Ya. Sokol, ZnO nanoparticles formation by reactions of bulk Zn with H_2O and CO_2 at sub- and supercritical conditions: II. Morphology and properties of nanoparticles, J. Supercritical Fluids 48 (2009) 161-166.

[32] B. Veriansyah, J.-D. Kim, B.K. Min, Y.H. Shin, Y.-W. Lee, J. Kim, Continuous synthesis of surface-modified zinc oxide nanoparticles in supercritical methanol, J. supercritical Fluids 52 (2010) 76-83.

[33] J. Zhang, S. Ohara, M. Umetsu, T. Naka, Y. Hatakeyama, T. Adschiri, Colloidal ceria nanocrystals: a tailor-made crystal morphology in supercritical water, Advanced Materials 19 (2007) 203-206.

[34] T. Arita, H. Hitaka, K. Minami, T. Naka, T. Adschiri, Synthesis and characterization of surface-modified FePt nanocrystals by supercritical hydrothermal method, Chemistry Letters 40 (2011) 588-590.

[35] T. Togashi, T. Naka, S. Asahina, K. Sato, S. Takami, T. Adschiri, Surfactant-assisted one-pot synthesis of superparamagnetic magnetite nanoparticle clusters with tunable cluster size and magnetic field sensitivity, Dalton Transactions 40 (2011) 1073-1078.

[36] T. Adschiri, Y.-W. Lee, M. Goto, S. Takami, Green materials synthesis with supercritical water, Green Chemistry 13 (2011) 1380-1390.

[37] F. Cansell, C. Aymonier, Design of functional nanostructured materials using supercritical fluids, J. Supercritical Fluids 47 (2009) 508-516.

[38] K. Byrappa, S. Ohara, T. Adschiri, Nanoparticles synthesis using supercritical fluid technology – towards biomedical applications, Advanced Drug Delivery Reviews 60 (2008) 299-327.

[39] T. Adschiri, Supercritical hydrothermal synthesis of organic–inorganic hybrid nanoparticles, Chemistry Letters 36 (2007) 1188-1193.

[40] E. Reverchon, R. Adami, Nanomaterials and supercritical fluids, J. Supercritical Fluids 37 (2006) 1-22.

[41] C. Aymonier, A. Loppinet-Serani, H. Reverón, Y. Garrabos, F. Cansell, Review of supercritical fluids in inorganic materials science, J. Supercritical Fluids 38 (2006) 242-251.

[42] J.R. Martínez, S. Palomares-Sánchez, G. Ortega-Zarzosa, F. Ruiz, Y. Chumakov, Rietveld refinement of amorphous SiO_2 prepared via sol–gel method, Materials Letters 60 (2006) 3526-3529.

[43] R. Göbel, A. Friedrich, A. Taubert, Tuning the phase behavior of ionic liquids in organically functionalized silica ionogels, Dalton Transactions 39 (2010) 603-611.

[44] Y.S. Chaudhary, J. Ghatak, U.M. Bhatta, D. Khushalani, One-step method for the self-assembly of metal nanoparticles onto facetted hollow silica tubes, J. Materials Chemistry 16 (2006) 3619-3623.

[45] Shell thickness is the average thickness calculated from 50 MARIMO TiO_2 nanoparticles from the TEM images.

[46] Details are shown in electronic supplementary data.

[47] D.A. Wright, D.A. Williams, The crystal and molecular structure of titanium tetramethoxide, Acta Crystallographica - Section B: Structural Crystallography & Crystal Chemistry 24 (1968) 1107-1714.

[48] J. Hu, M. Chen, X. Fang, L. Wu, Fabrication and application of inorganic hollow spheres, Chemical Society Reviews 40 (2011) 5472-5491.

[49] L. Ratke, P.W. Voorhees, Growth and Coarsening: Ostwald Ripening in Material Processing. Springer, 2002, pp. 117–118.

[50] The results will be published elsewhere shortly.